

Shear modulus and Dilatancy Softening in Granular Packings above Jamming.

C. Coulais,^{1,2,3} A. Seguin,^{1,2} and O. Dauchot⁴

¹*SPHYNX/SPEC, CEA-Saclay, URA 2464 CNRS, 91191 Gif-sur-Yvette, France*

²*Université Paris-Sud, CNRS, Lab FAST, Bat 502, Campus Université, Orsay, F-91405, France*

³*Kamerlingh Onnes Lab, Universiteit Leiden, Postbus 9504, 2300 RA Leiden, The Netherlands*

⁴*EC2M, ESPCI-ParisTech, UMR Gulliver 7083 CNRS, 75005 Paris, France*

We investigate experimentally the mechanical response of a monolayer of bi-disperse frictional grains to an inhomogeneous shear perturbation across the jamming transition. We inflate an intruder inside the packing and use photo-elasticity and tracking techniques to measure the induced shear strain and stresses at the grain scale. We quantify experimentally the constitutive relations for strain amplitudes as low as 10^{-3} and for a range of packing fractions within 2% variation around the jamming transition. At the transition strong nonlinear effects set in : both the shear modulus and the dilatancy shear-soften at small strain until a critical strain is reached where effective linearity is recovered. The dependencies of the critical strain and the associated critical stresses on the distance from jamming are extracted via scaling analysis. We check that the constitutive laws, when applied to the equations governing mechanical equilibrium, lead to the observed stress and strain profiles. These profiles exhibit a spatial crossover between an effective linear regime close to the inflator and the truly nonlinear regime away from it. The crossover length diverges at the jamming transition.

PACS numbers: 45.70.-n 83.80.Fg

Introduction — Understanding the mechanical properties of dense packings of athermal particles, such as grains, foams and emulsions, remains a conceptual and practical challenge. These intrinsically out-of-equilibrium systems lose their rigidity at the so-called jamming transition, which occurs at a packing fraction ϕ_J , when the confining pressure approaches zero and the particles deformations vanish [1–4]. The peculiarity of this transition is best illustrated in the case of frictionless spheres [2, 3], where the loss of mechanical stability occurs when the average number of contacts z reaches its isostatic value. Approaching the transition, the material becomes more and more fragile [5], and its linear response, dominated by floppy modes [6], exhibits critical scaling [2–4, 7].

In a first step towards the description of such systems, Wyart and coworkers [6, 8–10] derived, from a marginal stability principle, a scaling theory of the jamming transition that describes most of its phenomenology. In particular it predicts the existence of two length scales $\ell^* \sim 1/\Delta z$ and $\ell_c \sim 1/\Delta z^{1/2}$, where $\Delta z \sim \Delta\phi^\delta$ is the excess of contact with respect to isostaticity with $\Delta\phi = \phi - \phi_J$ and $\delta \simeq 0.5$. Recently, marginality has been translated into the adoption of a full replica symmetry breaking scheme in the formulation of a mean field theory of hard sphere glasses at high density [11–13]. As a result, the theory properly describes not only the thermodynamic properties of the packing, but also the structural and dynamical ones, when approaching ϕ_J .

However, the relevance of these theories for real systems remains to be established. There are very few direct experimental investigations of the scaling regime above jamming. The average number of contacts has been measured in grains [14, 15], foams [16] and emulsions [17] but not with a sufficient accuracy to provide stringent bounds for the value of the scaling exponent δ . As for

the dynamics and the mechanics, rheology below jamming has been studied in vibrated grains [18], foams [19] and emulsions [20], but we are not aware of any direct measurements of the elastic moduli dependence on the packing fraction when approaching jamming *from above*.

As a matter of fact, the relevance of the linear response very close to the transition actually remains a matter of debate [21–23]. At finite shear strain amplitude γ , non-linear effects become dominant [9, 24, 25] and the mechanical response of the system is no longer relevantly described exclusively by Δz but also by γ in a non-trivial way. Furthermore, most experiments using colloids are too hot for the constituents to experience marginality and henceforth to be described by jamming scalings [26, 27]. Finally, while dilatancy effects are dominant in sheared granular experiments [28–30], they are systematically missed in numerical and theoretical studies of soft spheres near jamming.

In this Letter, taking advantage of the possibility to probe jamming scalings in a weakly vibrated monolayer of soft grains [15, 26, 31], we provide the first experimental measurement of the elastic response of a 2D packing of grains across the jamming transition. To do so we apply an inhomogeneous shear by inflating an intruder in the center of a monolayer of bi-disperse frictional grains. We obtain the force network and grain displacements from photo-elasticity measurements and tracking techniques, thus allowing us to calculate the stress and strain tensors at the grain scale. The constitutive laws, obtained from a parametric plot of the invariants of the stress tensor with respect to the shear strain, reveal that linear elasticity does not apply. Dilatancy can never be neglected and, above jamming, we observe a shear softening regime at moderate strain. Elasticity is effectively recovered only for strains larger than a critical one. This shear softening regime scales with the distance to jamming and eventu-

ally vanishes at ϕ_J . We compute the strain profiles from the inferred constitutive laws and show that they match self-consistently the experimental profiles and display a spatial crossover between the two regimes. The crossover length diverges like $\Delta\phi^{-0.85}$ when the system (un)jams.

Setup and Protocol — The setup is adapted from [15, 31]. A bi-disperse layer of 8166 photo-elastic disks of diameter 4 and 5 mm is confined in a rectangular frame. The area of the system can be fine-tuned thanks to a wall piston, allowing to precisely tune the packing fraction ϕ . The grains lie on a glass plate that can be vibrated with an amplitude of 1 cm at a frequency of 10 Hz perpendicularly to the direction of the wall piston. The inflater is designed as follows: a brass spacer, equipped with 9 radial pistons, is surrounded by an O-ring of diameter $2r_I = 26.3$ mm and connected to a pressure switch. When the pressure is increased inside the spacer, the pistons push the O-ring radially, ensuring a uniform radial dilation, up to $2(r_I + a) = 28.5$ mm. When the pressure is switched off, the elasticity of the O-ring brings back the inflater to its initial diameter. The dilation rate $a^* = a/r_I$ ranges from 1 to 10%.

Varying both the strain amplitude and packing fraction, we record the stress response in each experiment following a precise protocol. First we introduce the inflater at the center of the packing at low packing fractions. We then compress the packing into a highly jammed state while vibrating the bottom plate (see [31] for details). We stop the vibration and start acquiring images while increasing the size of the intruder using steps of 1.5%. At the end, we let the inflater recover its initial size, turn on the vibration, stepwise decrease the packing fraction and start the next measurement loop.

The photo-elastic grains are backlit with a large, uniform, circularly polarized light source. Pictures are taken using a high-resolution CCD camera. We record both photo-elastic and position information by alternating between cross-polarized and direct pictures using a cross polarizer mounted on a synchronized step motor (see [31] for details). We process these images with standard segmentation, tracking and tessellation techniques, allowing us to reconstruct the displacement field, the force network. Ultimately, we compute the strain tensor ϵ and the stress tensor σ fields at the grain scale [29, 32, 33]. Having checked that these tensors are collinear, *i.e.* that they have the same eigenvectors [34], we can restrict the analysis to their first and second invariants: the dilatation $\varepsilon = \frac{1}{2}\epsilon_{kk}$, the pressure $P = -\frac{1}{2}\sigma_{kk}$, the shear strain $\gamma = \sqrt{\frac{3}{2}(\epsilon_{ij} - \varepsilon\delta_{ij})^2}$ and the shear stress $\tau = \sqrt{\frac{3}{2}(\sigma_{ij} + P\delta_{ij})^2}$ where δ_{ij} is the Kronecker symbol. In the following, P and τ are normalized by the contact stiffness $k = 1 \text{ Nmm}^{-1}$ and the length unit is the diameter of the small grains $s = 4$ mm.

Initial state — For each packing fraction, before inflating the intruder, the system is characterized by an initial state, with force chains spanning the whole system. This compressed state above jamming, which has been stud-

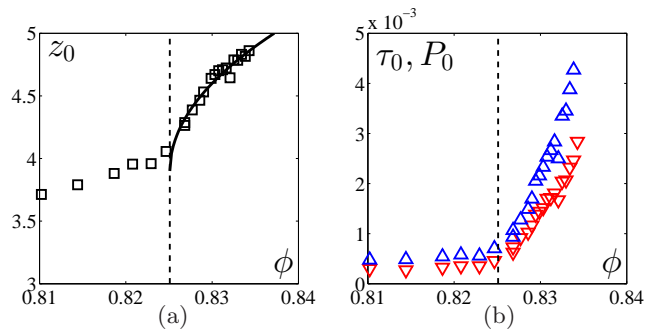


FIG. 1: **Initial stress state.** (color online) Initial average contact number (\square) z_0 (a), pressure (\triangle) P_0 and shear stress (∇) τ_0 (b) vs. packing fraction, ϕ . The solid line is a fit to $z_0 = z_p(\phi - \phi_J)^{0.5} + z_J$, with $\phi_J = 0.8251 \pm 0.0009$, $z_p = 10.0 \pm 0.5$, and $z_J = 3.9 \pm 0.1$. The dashed line indicates ϕ_J .

ied in detail before [31], is statistically homogeneous. The average contact number z_0 is essentially constant at low packing fraction (see fig. 1 a). At intermediate packing fraction, it exhibits a kink from where it increases sub linearly. By fitting to a square root power-law, we identify the location of the kink with the jamming transition at packing fraction $\phi_J = 0.8251 \pm 0.0009$. One should not be surprised to observe a finite z_0 below jamming: when the vibration is turned off, the structure is quenched abruptly from a vibrational state where the averaged number of contact need not be zero. The sub-linear increase of z_0 with packing fraction is compatible with the one obtained in simulations of frictional particles [16, 35]. The initial pressure P_0 also increases above jamming from a small residual value below jamming, again inherited from the vibrational state (see fig. 1-(b)). Also, since the packing is compressed by moving only one lateral wall, the compression is not isotropic. As a result, the packing conserves some anisotropy clearly evidenced by the existence of a residual shear stress τ_0 proportional to the pressure P_0 (see fig. 1-(b)). However the ratio τ_0/P_0 remains smaller than one, as expected for packings where compressive stresses dominate. Note that most numerical packing generation algorithms do not minimize shear and have residual shear stresses [36].

Response to inflation — Henceforth, we consider the excess of pressure P and shear stress τ produced while inflating the intruder: Stresses reported here are the difference between the stress measured at the initial state and those measured at each a^* . Assuming linear elasticity, $P = -K\varepsilon$ and $\tau = 2G\gamma$ (where K is the bulk modulus and G the shear modulus), it is straightforward to show that in an unconfined geometry, the inflation of a disk induces an azimuthally invariant shear, which decreases radially with the distance r from the center of the intruder $\tau \sim G\gamma \sim a^*/r^2$.

Figure 2 displays the four maps of the two strain (top row) and two stress (bottom row) invariants for a typical packing fraction above jamming and a typical a^* (4.4×10^{-2}). Apart from the spatial fluctuations inherent to the local response of a disordered material, one observes that the axisymmetry of the loading is conserved

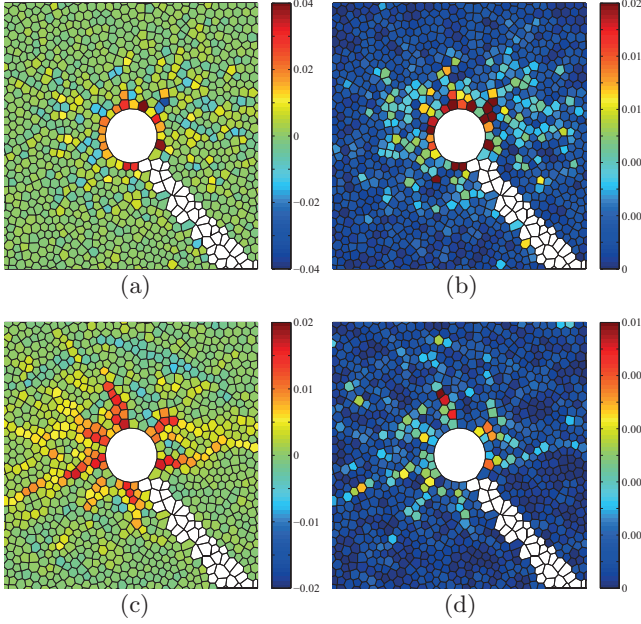


FIG. 2: **Maps of the strain and stress invariants.** (color online) Maps of dilation, ε , (a), shear strain, γ , (b), pressure, P , (c) and shear stress, τ , (d), for $\phi = 0.8294$ and $a^* = 4.4 \times 10^{-2}$. The uncolored grains sit below the pneumatic tube connected to the intruder, which masks the field of view.

in the response. Furthermore, the response intensity decreases with the distance from the intruder and we could observe no sign of the lateral walls. In other words, the hypothesis of an infinite cell is rather well verified (note that the images shown here represent only one third of the length of the whole sample). One notices that, apart from the very first shell around the inflator, the dilation ε fluctuates around 0 (fig. 2 a) : the material is essentially incompressible. This is confirmed by a closer look at the profile (not shown here) : close to the intruder a significant *dilation* occurs because of the boundary condition geometrical mismatch; but the rest of the packing compresses slightly and ensures the conservation of the overall volume. From now on, we shall remove the first shell around the intruder from the analysis and assume incompressibility, that is $\varepsilon = 0$. The second significant observation is that the pressure deviates significantly from the elastic response : there are regions of intense pressure, which do not correspond to any sort of intense compression. This pressure field is thus induced by the shear; it is the signature of dilatancy for an experiment conducted at constant volume, a well known effect in granular media [28]. Finally whereas the spatially averaged pressure varies linearly with a^* , the spatially averaged shear strain increases faster than a^* . This is a first indication of the nonlinear nature of the material. We checked however that the shear work $\tau\gamma$ averaged over space scales with a^{*2} . The above observations were qualitatively similar for all packing fractions.

Constitutive laws — We now come to the quantitative analysis of the constitutive laws $\tau(\gamma, \phi)$ and $P(\gamma, \phi)$ which were obtained from collecting all data points into

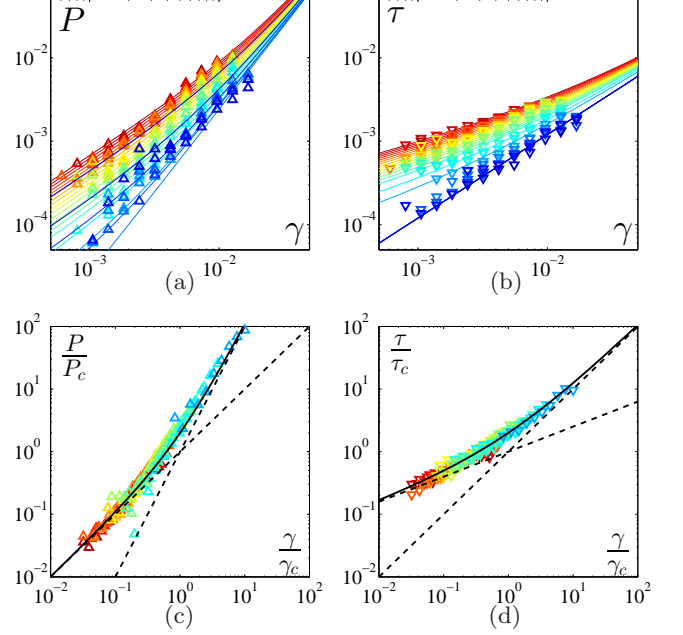


FIG. 3: **Constitutive laws.** (color online) Pressure, P (a), and shear stress, τ (b), vs. shear strain, γ , for 21 packing fractions $\phi \in [0.8102 - 0.8343]$. Each data point results from binning the scatter plots $P(r, \theta)$ and $\tau(r, \theta)$ vs. $\gamma(r, \theta)$, where (r, θ) are the polar coordinates. The solid lines are given by Eqs. (1-2). Color code spans from blue to red with increasing packing fractions. (c) and (d): same data as (a) and (b) rescaled by $\gamma_c(\phi)$, $P_c(\phi)$ and $\tau_c(\phi)$. The solid lines are given by the rescaled version of Eqs. (1-2) and the dashed lines indicate the asymptotic regimes.

averages corresponding to binned values of γ . Fig 3(a) and (b) display the shear stress τ and pressure P versus the shear strain γ for all the packing fractions probed. Below jamming, both the shear stress τ and the pressure P exhibit the simple expected dependence on the shear strain: $\tau = 2G_0\gamma$, and $P = R_0\gamma^2$. Above jamming nonlinearities take place in the form of a significant shear softening of both the shear modulus and the dilatancy. We find that the best description of the data is given by

$$P = [R_0 + R_{nl}(\Delta\phi, \gamma)] \gamma^2 \quad (1)$$

$$\tau = 2[G_0 + G_{nl}(\Delta\phi, \gamma)] \gamma \quad (2)$$

with $\Delta\phi = \phi - \phi_J$, $G_0 = 6.0 \pm 0.2 \times 10^{-2}$, $R_0 = 1.2 \pm 0.1 \times 10^1$ and

$$R_{nl}(\Delta\phi, \gamma) = \begin{cases} 0 & \text{for } \phi < \phi_J \\ a\Delta\phi^\mu\gamma^{\alpha-2} & \text{for } \phi > \phi_J \end{cases},$$

$$G_{nl}(\Delta\phi, \gamma) = \begin{cases} 0 & \text{for } \phi < \phi_J \\ b\Delta\phi^\nu\gamma^{\beta-1} & \text{for } \phi > \phi_J \end{cases},$$

with $\mu = 1.7 \pm 0.1$, $\alpha = 1.0 \pm 0.1$, $a = 8.1 \pm 0.3 \times 10^{-2}$, $\nu = 1.0 \pm 0.1$, $\beta = 0.4 \pm 0.1$, $b = 7.5 \pm 0.3 \times 10^{-1}$. From the above relations, one obtains the rescaling shown in figure 3(c),(d) with $\gamma_c \sim \Delta\phi^\zeta$, $\tau_c = 2G_0\gamma_c$ and $P_c = R_0\gamma_c^2$. Despite the fact that the exponent pairs (μ, α) and (ν, β) have been obtained independently, we find that

$\zeta = \mu/(2 - \alpha)$ and $\zeta = \nu/(1 - \beta)$ lead to the same value $\zeta = 1.7$, as it should be. The above equations and the related scaling are the key results of the present study. To our knowledge, this is the first time that non linear elasticity is quantified precisely approaching the jamming transition of a granular packing. Note that the "linear" regime observed here should not be confused with the linear response and should rather be seen as a saturation of the nonlinearities. For very small strain, ($\gamma \simeq 10^{-6}$), such as those probed in numerical studies [3, 36], and much smaller than the lowest strain probed here ($\gamma \simeq 10^{-3}$), one expects to recover a linear response for all $\Delta\phi > 0$ [23]. For strains of experimental relevance, very recent numerical studies have reported a crossover from the linear response at small strains to a shear softening regime, with a exponent $\beta \simeq 0.5$ [37, 38], compatible with the present results.

Shear strain profiles — We finally proceed to a self-consistency check by integrating the condition of mechanical equilibrium $\nabla \cdot \sigma = 0$, with the above constitutive laws to derive the expected shear strain profiles and compare them with those obtained experimentally. We introduce here the reduced shear strain $\tilde{\gamma} = \gamma/\gamma_c$. Axisymmetry ensures that σ is diagonal in polar coordinate and independent of the azimuthal coordinate θ . $\nabla \cdot \sigma = 0$ thus reads:

$$\frac{P_c(\alpha\tilde{\gamma}^{\alpha-1} + 2\tilde{\gamma}) + \tau_c(\beta\tilde{\gamma}^{\beta-1} + 1)}{\tilde{\gamma}^\beta + \tilde{\gamma}} d\tilde{\gamma} = -2\tau_c \frac{dr}{r} \quad (3)$$

We numerically integrate Eq. 3 with the boundary condition $\tilde{\gamma}(r = r_I) = a^*/\gamma_c$ and we obtain the profiles plotted in figure 4(a), together with the experimental data. The agreement is excellent, given the absence of any adjustable parameter and the fact that we have neglected the confinement at large r . For intermediate values of $\Delta\phi$ and a^* , the crossover of the constitutive law translates into a spatial crossover with a characteristic length r_c between the saturated linear regime for $r < r_c$, close to the inflator, and the truly non linear regime for $r > r_c$. An estimate of r_c can be derived by integrating the above equation in the saturated linear regime and selecting $\gamma = \gamma_c$ ($\tilde{\gamma} = 1$) :

$$\frac{r_c}{r_I} = \left(\frac{a^*}{\gamma_c}\right)^{1/2} \exp\left[\frac{R_0}{2G_0} a^* \left(1 - \frac{\gamma_c}{a^*}\right)\right]. \quad (4)$$

In the limit, $\gamma_c \rightarrow 0$, approaching jamming, $r_c \sim \gamma_c^{-1/2} \sim \Delta\phi^{-0.85}$. One can indeed observe the emergence of this singular behavior on figure 4(b), together with the exponential regularization at large $\Delta\phi$.

Summary-Discussion — Our measurements provide a quantitative characterization of the elastic response of a 2D packing of grains to the local inflation of an intruder close to jamming. This specific geometry actually probes the response to an inhomogeneous shear at constant volume. Our results highlight the effect of dilatancy and

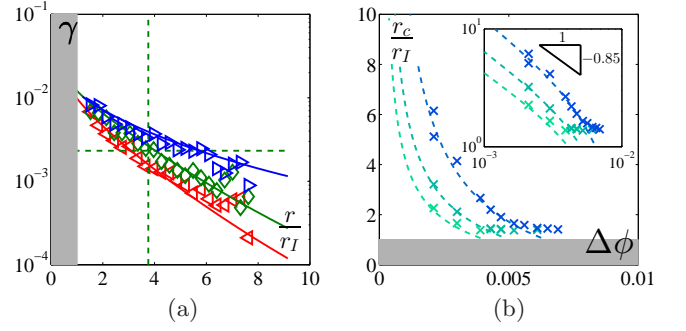


FIG. 4: **Shear strain profiles** (color online) **(a)**: Shear strain profile for (\triangleright) ($\phi = 0.8208$; $a^* = 0.0374$), (\diamond) ($\phi = 0.8268$; $a^* = 0.0314$) and (\triangleleft) ($\phi = 0.8338$; $a^* = 0.0306$). The symbols are experimental data and the solid lines come from the integration of eq.(3). The green dashed line indicates the crossover for the case ($\phi = 0.8268$; $a^* = 0.0314$) **(b)**: Spatial crossover $r_c(\phi, a^*)/r_I$ (for $a^* = 0.0208$ (green), 0.0440 (turquoise) and 0.0681 (blue) extracted from the experimental profiles (\times) and obtained numerically from eq. (3) (dashed lines). **(Inset)**: same in log-log axis with the predicted scaling $r_c \sim \Delta\phi^{-0.85}$. In both figures, the gray zone is the region occupied by the inflator.

unveil a nonlinear regime above jamming where both the shear modulus and the dilatancy coefficient soften. The importance of shear dilatancy in marginal solids was recently emphasized in [39], where it was shown that the Reynolds coefficient at constant volume R_V scales like $\Delta\phi^{-1/2}$. Here we also observe a singular behavior, albeit of a different kind since the present experiment probes the nonlinear softening of the dilatancy. In a different context, Ren et al. [30] report a steep increase of dilatancy under homogeneous shear as the density of an unjammed packing of grains is increased. The dilatancy coefficient R_0 reported here is indeed very large ($R_0 \sim 10^4$ N/m) and could be seen as a saturation of the divergence reported in [30].

Finally, the present study uncovers a length scale, r_c , which separates the nonlinear regime from the saturated linear one. Its scaling with the distance to jamming does not match any scaling reported before for length scales of linear origin, such as ℓ^* or ℓ_c . This suggests that r_c could encompass crucial information about the density of the low energy non-linear excitations reported recently for sphere packings [24]. Further insights in this matter could come from simulations of point-like response of the kind reported in [7] albeit in the non linear regime.

Acknowledgements — We thank B. Tighe, W. Ellenbroek and M. van Hecke for discussions. We are grateful to V. Padilla and C. Wiertel-Gasquet for their skillful technical assistance. This work is supported by the ANR project STABINGRAM No. 2010-BLAN-0927-01 and RTRA Triangle de la Physique project REMIGS2D.

-
- [1] A. J. Liu and S. R. Nagel, *Nature* **396**, 21 (1998).
 - [2] C. S. O'Hern, S. A. Langer, A. J. Liu, and S. R. Nagel, *Phys. Rev. Lett.* **88**, 075507 (2002).
 - [3] C. S. O'Hern, L. E. Silbert, A. J. Liu, and S. R. Nagel, *Phys. Rev. E* **68**, 011306 (2003).
 - [4] M. van Hecke, *Journal of Physics: Condensed Matter* **22**, 033101 (2010).
 - [5] M. E. Cates, J. P. Wittmer, J.-P. Bouchaud, and P. Claudin, *Phys. Rev. Lett.* **81**, 1841 (1998).
 - [6] M. Wyart, S. R. Nagel, and T. A. Witten, *EPL (Europhysics Letters)* **72**, 486 (2005).
 - [7] W. G. Ellenbroek, E. Somfai, M. van Hecke, and W. van Saarloos, *Phys. Rev. Lett.* **97**, 258001 (2006).
 - [8] M. Wyart, L. E. Silbert, S. R. Nagel, and T. A. Witten, *Phys. Rev. E* **72**, 051306 (2005).
 - [9] C. Brito, O. Dauchot, G. Biroli, and J.-P. Bouchaud, *Soft Matter* **6**, 3013 (2010).
 - [10] N. Xu, V. Vitelli, M. Wyart, A. J. Liu, and S. R. Nagel, *Phys. Rev. Lett.* **102**, 038001 (2009).
 - [11] G. Parisi and F. Zamponi, *Rev. Mod. Phys.* **82**, 789 (2010).
 - [12] L. Berthier, H. Jacquin, and F. Zamponi, *Phys. Rev. E* **84**, 051103 (2011).
 - [13] P. Charbonneau, J. Kurchan, G. Parisi, P. Urbani, and F. Zamponi (2013), arXiv: 1310.2549.
 - [14] T. S. Majmudar, M. Sperl, S. Luding, and R. P. Behringer, *Phys. Rev. Lett.* **98**, 058001 (2007).
 - [15] C. Coulais, R. P. Behringer, and O. Dauchot, *EPL (Europhysics Letters)* **100**, 44005 (2012).
 - [16] G. Katgert and M. van Hecke, *EPL (Europhysics Letters)* **92**, 34002 (2010).
 - [17] I. Jorjadze, L.-L. Pontani, and J. Brujic, *Phys. Rev. Lett.* **110**, 048302 (2013).
 - [18] J. A. Dijksman, G. H. Wortel, L. T. H. van Dellen, O. Dauchot, and M. van Hecke, *Phys. Rev. Lett.* **107**, 108303 (2011).
 - [19] G. Katgert, B. P. Tighe, and M. van Hecke, *Soft Matter* **9**, 9739 (2013).
 - [20] V. Mansard and A. Colin, *Soft Matter* **8**, 4025 (2012).
 - [21] C. F. Schreck, T. Bertrand, C. S. O'Hern, and M. D. Shattuck, *Phys. Rev. Lett.* **107**, 078301 (2011).
 - [22] T. Bertrand, C. F. Schreck, C. S. O'Hern, and M. D. Shattuck (2013), arXiv: 1307.0440.
 - [23] C. P. Goodrich, A. J. Liu, and S. R. Nagel (2014), arXiv: 1402.6206.
 - [24] E. Lerner, G. During, and M. Wyart, *Soft Matter* **9**, 8252 (2013).
 - [25] L. R. Gomez, A. M. Turner, M. van Hecke, , and V. Vitelli, *Phys. Rev. Lett.* **108**, 058001 (2012).
 - [26] A. Ikeda, L. Berthier, and G. Biroli, *The Journal of Chemical Physics* **138**, 12A507 (pages 17) (2013).
 - [27] A. Basu, Y. Xu, T. Still, P. E. Arratia, Z. Zhang, K. N. Nordstrom, J. M. Rieser, J. P. Gollub, D. J. Durian, and A. G. Yodh, *Soft Matter* pp. – (2014).
 - [28] O. Reynolds, *The London, Edinburgh, and Dublin Philosophical Magazine and Journal of Science* **20**, 469 (1885).
 - [29] D. Bi, J. Zhang, B. Chakraborty, and R. P. Behringer, *Nature* **480**, 355 (2011).
 - [30] J. Ren, J. A. Dijksman, and R. P. Behringer, *Phys. Rev. Lett.* **110**, 018302 (2013).
 - [31] C. Coulais, R. P. Behringer, and O. Dauchot, *Soft Matter* **10**, 1519 (2014).
 - [32] A. Drescher and G. de Josselin de Jong, *Journal of the Mechanics and Physics of Solids* **20**, 337 (1972), ISSN 0022-5096.
 - [33] P. Cundall, A. Drescher, and O. Strack, *Proc. IUTAM* pp. 355–370 (1982).
 - [34] P.-P. Cortet, D. Bonamy, F. Daviaud, O. Dauchot, B. Dubrulle, and M. Renouf, *EPL (Europhysics Letters)* **88**, 14001 (2009).
 - [35] E. Somfai, M. van Hecke, W. G. Ellenbroek, K. Shundyak, and W. van Saarloos, *Phys. Rev. E* **75**, 020301 (2007).
 - [36] S. Dagois-Bohy, B. P. Tighe, J. Simon, S. Henkes, and M. van Hecke, *Phys. Rev. Lett.* **109**, 095703 (2012).
 - [37] M. Otsuki and H. Hayakawa (2014), arXiv: 1402.6473.
 - [38] B. P. Tighe, priv. comm.
 - [39] B. P. Tighe (2013), arXiv: 1305.5574.